Journal of Alloys and Compounds 735 (2018) 2111–2118

Contents lists available at ScienceDirect

Journal of Alloys and Compounds

journal homepage: http://www.elsevier.com/locate/jalcom

Magneto-dielectric properties studies of the matrix composite [$SrFe_{12}O_{19}(SFO)_{1-X} - BiFeO_3(BFO)_X$]

J.E.V. de Morais [a, b, *], R.G.M. Oliveira [a, b], M.A.S. Silva [b], M.M. Costa [c], A.J.M. Sales [a, b], V.L. Bessa [b], A.R. Rodrigues [d], I.F. Vasconcelos [f], J. Goldsmith [e], T.K. Carroll [e], A.S.B. Sombra [b]

[a] Telecommunication Engineering Department, Federal University of Ceará (UFC), P.O. Box 6007, Fortaleza, Ceará 60755-640, Brazil
[b] Physics Department - Telecommunication, Science and Engineering of Materials Laboratory (LOCEM), Federal University of Ceará (UFC), P.O. Box 6030, Fortaleza, Ceará, 60455-760, Brazil[1]
[c] Institute of Physics, LACANM, UFMT, 78060-900 Cuiabá, MT, Brazil
[d] Physics Department-Federal University of Pernambuco (UFPe), Brazil
[e] Sensors Directorate, Air Force Research Laboratory, Wright-Patterson AFB, OH, USA
[f] Materials Engineering Department, Federal University of Ceará (UFC), Brazil

ARTICLE INFO

Article history:
Received 13 June 2017
Received in revised form
9 October 2017
Accepted 8 November 2017
Available online 2 December 2017

Keywords:
Impedance spectroscopy
Mössbauer
Magnetic properties
Ferrites

ABSTRACT

The effects of different $BiFeO_3$ (BFO) additions (0, 20, 40, 60 and 80 wt%) on the $SrFe_{12}O_{19}$ hexaferrite ceramic matrix (SFO) have been studied by Complex Impedance Spectroscopy (CIS), Mössbauer spectroscopy, magnetic hysteresis and X-Ray Diffraction (XRD) analysis. The solid state reaction method was used for the production of the SFO and BFO, the phase formation was confirmed by the XRD and Rietveld refinement, where the obtained fitting presented an effective refinement. The diffractogram for BFO-SFO composites presented all peaks in agreement with the BFO and SFO phases. The thermo-activated process was studied by the CIS and the Arrhenius equation in the composite series of BFO-SFO with SFO presenting higher values of activation energy between the analyzed samples and the frequency and temperature range studied was 1–10 MHz and 160 °C to 300 °C, respectively. The addition of BFO in the SFO ceramic matrix lead to an improvement of the thermal-stability of the composite, where a signal inversion of Temperature Coefficient of Capacitance (TCC), in the composites, was observed. The Nyquist plots showed the presence of a semicircle that was fitted by an equivalent circuit model using R - CPE association, showing the same profile in all samples. The Mössbauer spectrum of the composites demonstrate the typical five Fe^{3+} site for M-type hexagonal ferrites even after the addition of BFO in a ceramic matrix. The addition of BFO in the formation of composites, with SFO, showed interesting results in the radio frequency range and presented magnetic properties that can be explored in applications in the area of telecommunications, medicine and military industry.

1. Introduction

Increased understanding of the correlation of magnetic phenomena with electricity has led to the discovery of new and important magnetic materials. These materials are used in the development of new technologies, such as power generation and distribution systems, aeronautics, electromechanical conversion systems, telecommunications, industrial automation, the medical field etc [1].

Ferrimagnetic materials as the hexagonal-type ferrites can combine the magnetic and insulating properties adequate for these types of applications [2,3]. Ferrite structure of the hexagonal-type may present the general chemical formula $MFe_{12}O_{19}$, where M site can be divalent ion with high coordination number (CN) equal to 12. The most common hexagonal ferrites are with M = Ba or Sr. The $SrFe_{12}O_{19}$ (SFO) is classified as hard magnet [4], high dielectric constant in radiofrequency ($\varepsilon_r > 100$) [5] and temperature coefficient of resonant frequency $\tau_f = 44.90$ ppm °C^{-1} [6]. The SFO is applied in device operation at radiofrequency and microwave

* Corresponding author.Telecommunication Engineering Department, Federal University of Ceará (UFC), P.O. Box 6007, Fortaleza, Ceará 60755-640, Brazil.
E-mail address: eduardovasconc@gmail.com (J.E.V. de Morais).
[1] http://www.locem.ufc.br.

https://doi.org/10.1016/j.jallcom.2017.11.116
0925-8388/

range, as radar detection, antennas etc [5,7–11]. Hexagonal ferrites absorb microwave energy due to high permeability, high saturation magnetization and anisotropic planar behavior at high frequencies. For new applications some desired properties (dielectric, magnetic or mechanical for example) are necessary, so the research for new materials by development of new structures (polymeric, ceramic, glass, etc) or mixture of phases which achieve the desired properties has been growing in the last decade [12]. Research aimed in obtaining materials with better performances and differentiated characteristics has been intensifying in recent years. The great demand for more thermal-stability materials of relevant technological interest had led to the development of advanced alloys and composites [12–14]. Dielectric properties with temperature stability can achieved by manipulation of crystalline lattice [15,16] or to change the formulation of composites, where the phases present in composite must present dielectric behavior opposite to each other [17–20]. The temperature coefficient in dielectric study can be resumed in follows Equation (1) [21]:

$$\tau_f = -\alpha_l - \frac{\tau_\varepsilon}{2} \quad (1)$$

where τ_f is the temperature coefficient for dielectric properties in microwave range, α_l is linear dilatation coefficient and temperature coefficient of permittivity (τ_ε) is the temperature coefficient for dielectric at radio frequency range for the material in study. In general, by Equation (1) is possible to estimate the signal of τ_ε for SFO, as the τ_f is positive was expected that signal of τ_ε will negative. To have an improvement of thermal-stability of SFO, is possible to build a composite formulated by other ceramic phase that present opposite properties, i.e., the ceramic phase must present positive τ_ε increasing the thermal-stability of ceramic composite. The $BiFeO_3$ (BFO) is a popular multiferroic ceramic [22,23], this ceramic presents high dielectric permittivity in the radiofrequency and microwave range ($\varepsilon r = 4.5.10^5$ [22], and $\varepsilon r = 24.8$ [24]) and τf around -269 ppm $°C^{-1}$ [24]. By Equation (1) can expressed that the signal of $\tau\varepsilon$ is positive, it can be a better candidate for improvement of thermal-stability of SFO. Moreover, the BFO can attributed multiferroic properties to composite.

In this work the formation of a new composite formed by the $SrFe_{12}O_{19}$ (SFO) strontium hexaferrite and the $BiFeO_3$ ferrite (BFO) in proportions ranging from 20, 40, 60 and 80 wt% are studied. For the validation of this composite, a study was conducted to analyze the response of this material in the radiofrequency and microwave range, as well as its electrical, dielectric and magnetic properties.

2. Experimental procedure

The synthesis of the $SrFe_{12}O_{19}$ was performed by solid state reaction, where the quantities of precursors utilized were calculated by stoichiometry of Equation (2), utilizing $SrCO_3$ (99%, Aldrich) and Fe_2O_3 (97%, Vetec) as reagents. After milling in the Planetary mill, on a Fritsch Pulverisette 6, for 1 h with stainless steel balls and steel jars, the powder was calcined in an air atmosphere at 1000 °C for 24 h. During the calcination reactions occurred forming the phase:

$$SrCO_3 + 6Fe_2O_3 \rightarrow SrFe_{12}O_{19} + CO_2 \quad (2)$$

The stoichiometric mixture of Bi_2O_3 (99.9%, Aldrich) and Fe_2O_3(97%, Vertec) was used in the preparation of $BiFeO_3$ (BFO) according to Equation (3), the milling process utilized in BFO's synthesis was same that utilized in SFO's synthesis, moreover the calcination process was at 750 °C for 3 h for the formation of the phase.

$$Bi_2O_3 + Fe_2O_3 \rightarrow 2BiFeO_3 \quad (3)$$

They were blended in SFO mass with 20, 40, 60, 80, wt% BFO using PVA as a binder for the formation of the composites. Ceramic pellets and cylinders were prepared for the dielectric measurements of the samples. Thus the powder of the composites were molded into a steel form and pressed into a uniaxial press with 200 MPa and sintered at 900 °C for 5 h. The crystal structure and composition were analyzed by X-ray diffraction (XRD, bruker) using CuKα radiation (λ = 0.15406 Å). For analysis of impedance spectroscopy the pellets were polished and each face painted with conductive silver to form a parallel face capacitor and placed in the oven at 500 °C for 1 h for drying. In order to obtain the impedance spectroscopy data, an impedance analyzer (Solartron 1260) was used. To perform the measurements of magnetization at room temperature a VSM (Vibrating Sample Magnetometer) equipment model EV7 with a sensitivity of 10^{-6} emu MicroSense was used. This tool offers great precision for measuring magnetic force. Room temperature Mössbauer spectra were acquired in transmission mode using a $^{57}Co(Rh)$ radioactive source mounted on a velocity driver operating in sinusoidal mode. The data were evaluated by least square fitting to series of discrete Lorentzian shaped subspectra by means of the software package Normos. Isomer shifts are quoted with respect to α-Fe.

3. Results and discussion

Confirmation of the $BiFeO_3$ (BFO) and $SrFe_{12}O_{19}$ (SFO) syntheses after the calcination step was performed by XRD and confirmed by quantitative analysis of the Rietveld method. Parameters such as Quality factor (S), weighted residual error (R_{WP}), Durbin - Watson statistics (R_{DW}) showed that the SFO and BFO refinement results were satisfactory for a good refinement. For the BFO, Fig. 1a, the diffraction peaks were identified with the reference standard ICSD - 15299 and the result was $R_{WP} = 14.11\%$, $S = 1.37$ and $R_{DW} = 1.24$. The BFO was refined by a rhombohedral structure ($R3c$ – space group) and present density of the 8.36 g cm^{-3} for a BFO monocrystal. For the SFO, Fig. 1f, the peaks were identified with the reference standard ICSD - 202518 and the refinement results was $R_{WP} = 16.39\%$, $S = 1.07$ and $R_{WD} = 1.58$. The patterns diffraction was refined by hexagonal structure ($P6_3/mmc$ -space group) and present density of 5.38 g cm^{-3} for a SFO monocrystal. All peaks in the added samples, Fig. 1b, c, 1d and 1e were in agreement with all the peaks of BFO and SFO, without a spurious phase in diffractograms [25].

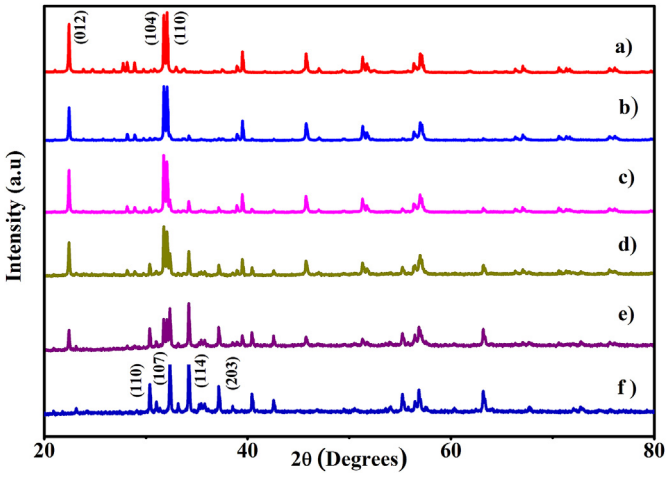

Fig. 1. XRD pattern for: a) SFO, b) SB20, c) SB40, d) SB60 e) SB80 and f) BFO.

The impedance measurements used characterize the dielectric behavior of materials and showed an interesting tool to describe the electrical behavior of the ceramic materials. Fig. 2 shows the electrical conductivity as a function of the frequency and temperature for the samples SFO, SB20, SB40 and S60. In these spectra is possible to see that all samples at all temperatures analyzed present a dispersion in relation to the frequency. Also in these spectra is possible to observe that the independent behavior of conductivity (1 Hz to 1 kHz) can be associated with dc conduction. These ferrites behave like a multilayer capacitor, in which the ferrite samples are characterized by a microstructure consisting of thick conductive grains, the grains separated by thin resistive layers, the grain boundary. The impedance is represented by Equation (4).

$$Z = R + \frac{1}{j\omega C} \tag{4}$$

where ω is the angular frequency and R, C are the resistance and capacitance presented by the material, respectively. In the measurements were observed that the admittance ($Y = Z^{-1}$) increases with the conductivity of the ferrite, frequency and temperature [26]. This increase can be attributed to changes in the mobility and hopper frequency of load carriers with increasing temperature. The linear profile obtained by plots of ln (σ or $f_{z''max}$) versus inverse of absolute temperature follows the Arrhenius equation for thermo-activated processes, see Equations (5) and (6) [27].

$$\sigma = \sigma_0 e^{\frac{-Ea}{kT}} \tag{5}$$

$$f_{Z''_{max}} = f_0 e^{-EakT} \tag{6}$$

where σ is the conductivity, σ_0 and f_0 are pre-exponential factors, Ea is the activation energy for thermo-activated processes, $f_{Z''max}$ is maximum peak frequency of imaginary impedance, k is a Boltzmann's constant and T is absolute temperature. Table 1 shows the activation energy values (Ea) of the SFO-BFO composites obtained by conductivity and Z". The fact that these values are close, show that the thermo-activated process observed in both measurements are the same. The SFO sample presents higher Ea (0.78 eV) into all analyzed samples. The BFO addition present smaller values and the composites present smaller values than BFO (0.62–0.67 eV) demonstrating the higher conductive character relative to the main phases. The behavior of the Ea for the composites compared to the pure phases can be explained most likely due to defects caused in the sinterization process of composites above of the temperature commonly founded in literature for BFO ceramic [28].

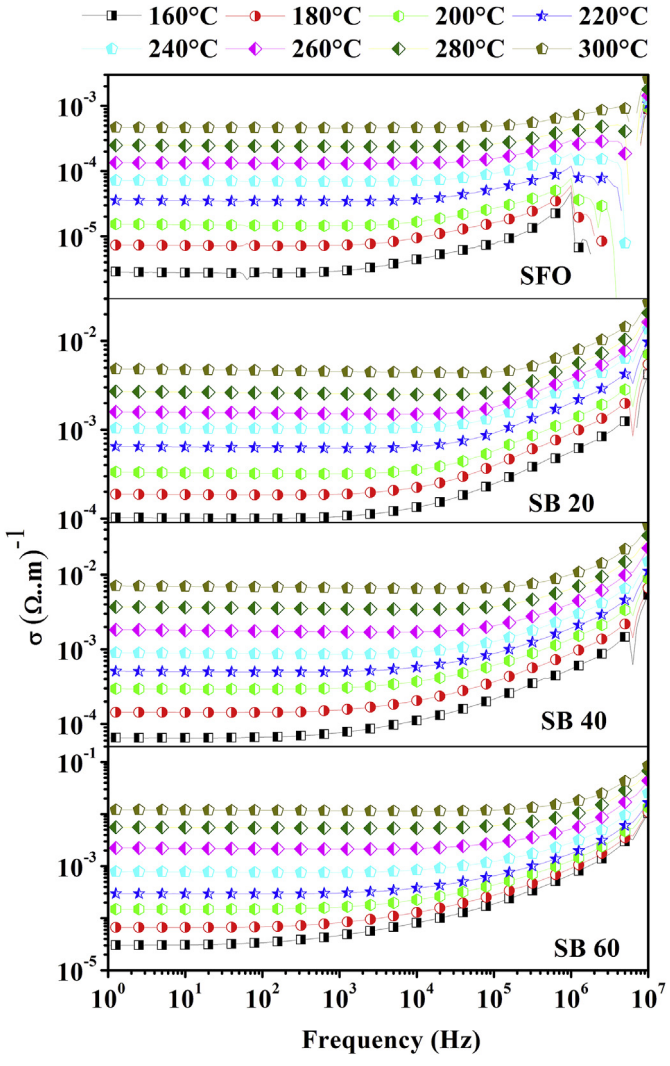

Fig. 2. Conductivity measurement for the SFO, SB20, SB40 and SB60 samples.

The thermo-activated process can be seen in Fig. 3 where it shows the variation of the imaginary part of the modulus (M″) normalized with the frequency at temperatures of 160 °C–300 °C in which a peak of relaxation observed that can be attributed to the conduction mechanism [29]. It can be verified that there is a relaxation frequency shift with increasing of the temperature. Also the BFO addition caused the frequency shift of relaxation peak, where all samples BFO-added showed higher frequencies for relaxation process than the SFO sample. For BFO M″ spectrum the peak relaxation it is located above the analyzed frequency range in this work. All composites analyzed show the relaxation process with frequency higher than SFO and lower than BFO. Also, is seen little profile variation of composite's M″ spectra, this observation can be explained by higher BFO molar concentrations in the composites, that despite having higher mass concentrations of SFO presents smaller molar concentrations, i.e., to mass composition used in this work (20, 40, 60 and 80%wt) it's equivalent to molar composition 42.38, 66.24, 81.53 and 92.15% of the BFO in composite respectively, increasing molar concentration of BFO increased the composites relaxation frequency. The frequency dependence on the real and imaginary part of the impedance at different temperatures is shown in Figs. 4 and 5 respectively. For this analysis, the SFO, SB20, SB40 and SB60 are shown. It can be seen that the real part of the impedance for the samples show a region independent of the frequency 1 Hz - 10^3 Hz. This independent frequency region increases with the temperature. Large values of Z′ at low frequencies indicate a predominant polarization effect as seen in all samples [30]. The real part impedance decreases with increasing frequency for all samples indicating an increase in conductivity. The junction

Table 1
Activation energy and temperature coefficient of capacitance (TCC).

Activation Energy of the composites SFO - BFO			TCC (ppm.°C^{-1})	
Sample	Ea_σ(eV)	$E_{aZ''}$ (eV)	100 Hz	10 KHz
SFO	0.78	0.78	−446.43	−136.05
SB20	0.62	0.57	45412.31	15707.52
SB40	0.64	0.65	46638.65	24520.91
SB60	0.66	0.66	41217.80	10776.94
SB80	0.67	0.66	58301.16	11111.11
BFO	0.68	0.71	26769.02	25247.08

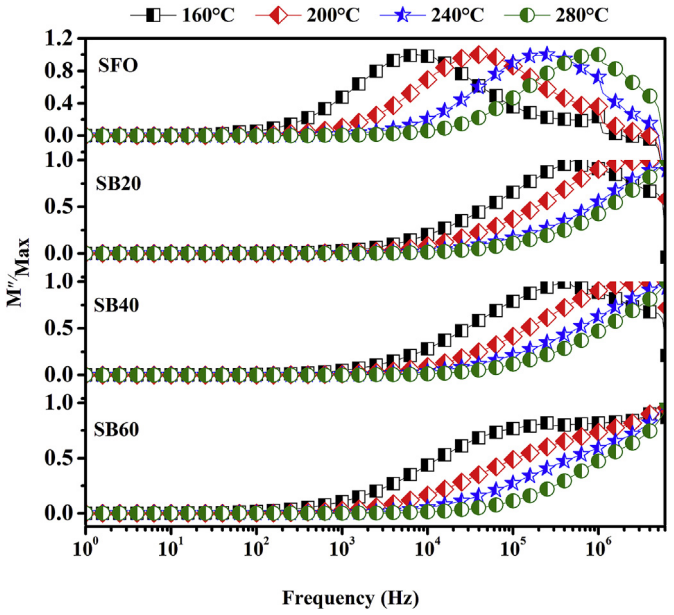

Fig. 3. Normalized imaginary part of the modulus (M″) as a function of frequency at different temperatures for SFO, SB20, SB40 and SB60.

of the real part of the impedance to high frequencies suggests the release of spatial charges with the decrease of the energy barrier [31]. It was observed that the addition of BFO in the SFO decreases the real impedance values. In the spectra of Z″, Fig. 5, show a relaxation region where there is a peak shift to high frequencies with increasing temperature. This behavior occurs for all samples, indicating conduction related to the reorientation of the dipoles.

The TCC values measured in the CIS study reveals an improvement of thermal-stability of dielectric properties of composites with the increase of BFO concentrations, according to Table 1, as expected the signal of TCC was inverted with BFO concentrations. The TCC calculated show the values close to zero for BFO concentrations below to 20%wt.

Fig. 6 shows the Nyquist diagram for sample SB40. The measured impedance shows the presence of a semicircle where they were adjusted by equivalent circuit model and the impedance of the circuit composed of resistor and constant phase element (CPE) is given by Equation (7).

$$Z(\omega) = \frac{1}{R^{-1} + p\omega^{n}\left(\cos\frac{\pi}{2}n\right) + isen\left(\frac{\pi}{2}n\right)} \tag{7}$$

where p is a proportionality factor (capacitance equivalence), and n is the CPE exponent that characterizes the phase shift and R is the resistance [31]. The presence of arcs modeled by Equation (7) indicates the electric response of grain, grain boundary and electrode effect in impedance measurements of electroceramics. The elements were modeled by an R - CPE circuit that represents practically the same behavior in all samples. In Table 2 was observed that the resistance decrease with increasing temperature, the conduction process activated by temperature of the material can explain this phenomenon. The factor “n” founded in the fitting of Nyquist plot is in the range 0.4 < n < 0.6, this values of the CPE is related to diffusion, with deviations from Fick's second law [32]. As n is

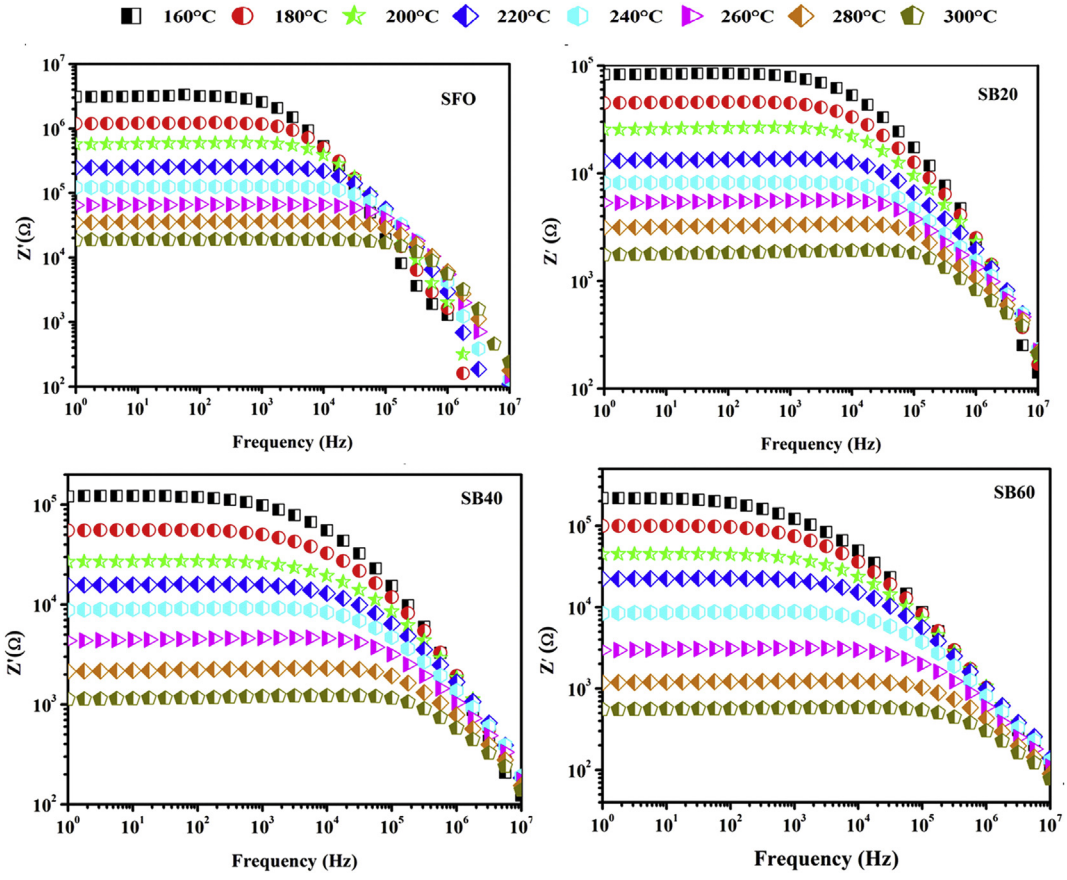

Fig. 4. Frequency dependence of Z′ with frequency at different temperatures.

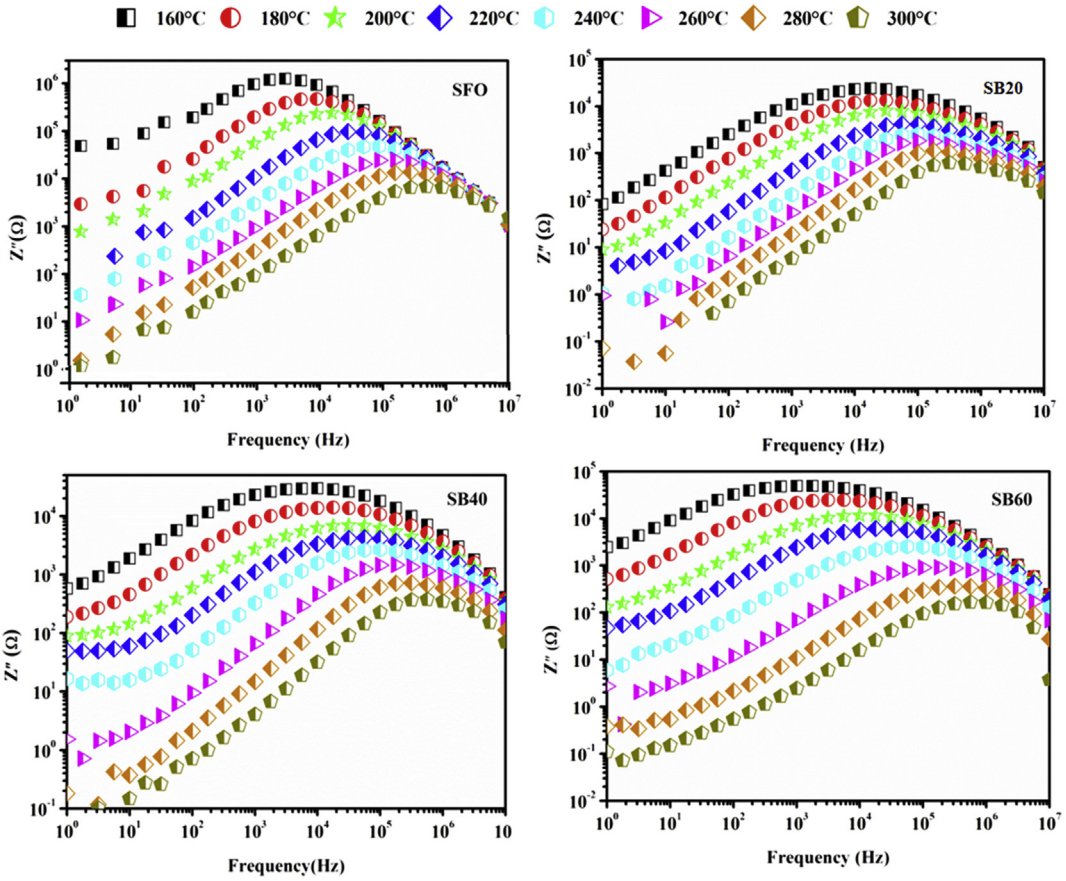

Fig. 5. Frequency dependence of Z″ with frequency at different temperatures.

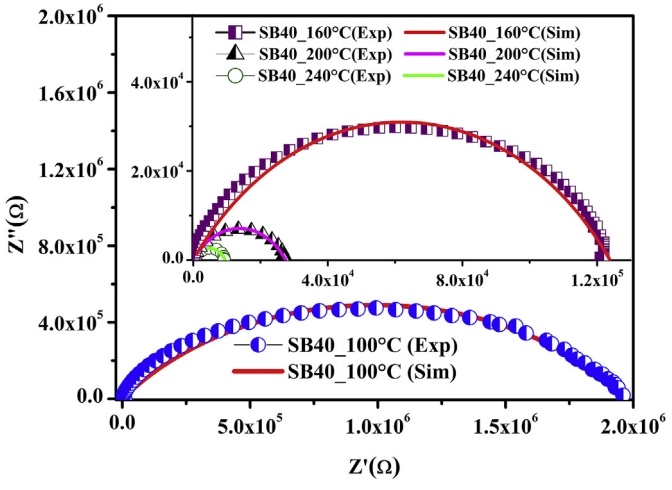

Fig. 6. Nyquist diagram for SB40 sample at different temperatures.

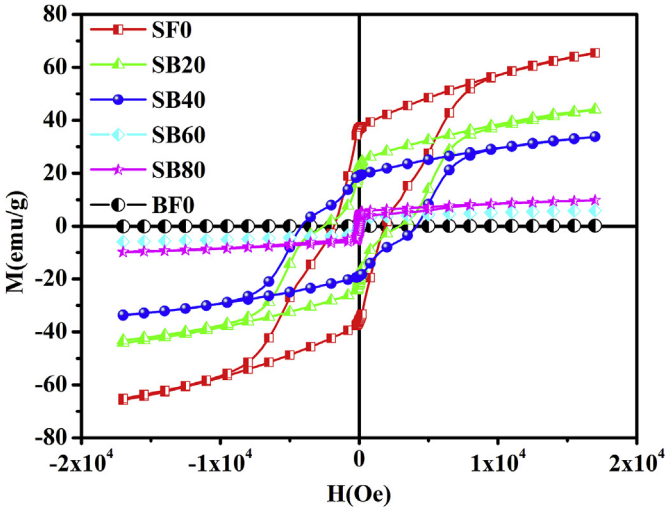

Fig. 7. Hysteresis loop for samples SFO, SB20, SB40, SB60, SB80 and BFO.

Table 2
Fitting of equivalent circuit parameters for SB40.

	$R_1(\Omega)$	P_1	n_1	τ(ms)
SB40_100	$1.97\cdot10^{6}$	$5.83\cdot10^{-9}$	0.587	11.49
SB40_160	$1.24\cdot10^{5}$	$1.47\cdot10^{-8}$	0.591	1.82
SB40_200	$2.75\cdot10^{4}$	$2.17\cdot10^{-8}$	0.607	0.60
SB40_240	$9.48\cdot10^{3}$	$1.74\cdot10^{-8}$	0.652	0.16

Table 3
Properties obtained from hysteresis loop for each sample.

	SFO	SB20	SB40	SB60	SB80	BFO
Hc(Oe)	−1814.18	−2501.52	−4132.33	−11	−31	–
Mr(emu/g)	36.79	20.98	18.89	0.30	2.11	–
Ms(emu/g)	65.33	43.89	33.46	5.85	9.62	–

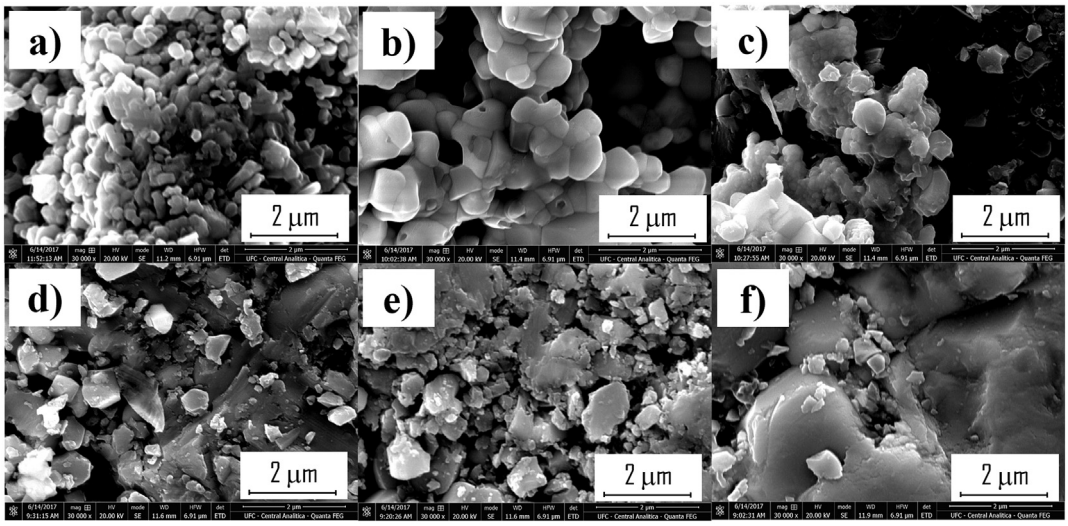

Fig. 8. SEM of SFO and composites. a) SFO, b) SB20, c) SB40, d) SB60 e) SB80 and f) BFO.

increasing with temperature variation and some of the factors that may be contributing to this are the surface of the electrode, thickness or composition of the sample, non-uniform current distribution among other factors.

Fig. 7 shows the hysteresis loop of samples at room temperature the magnetization of the SFO, BFO and composites in compositions

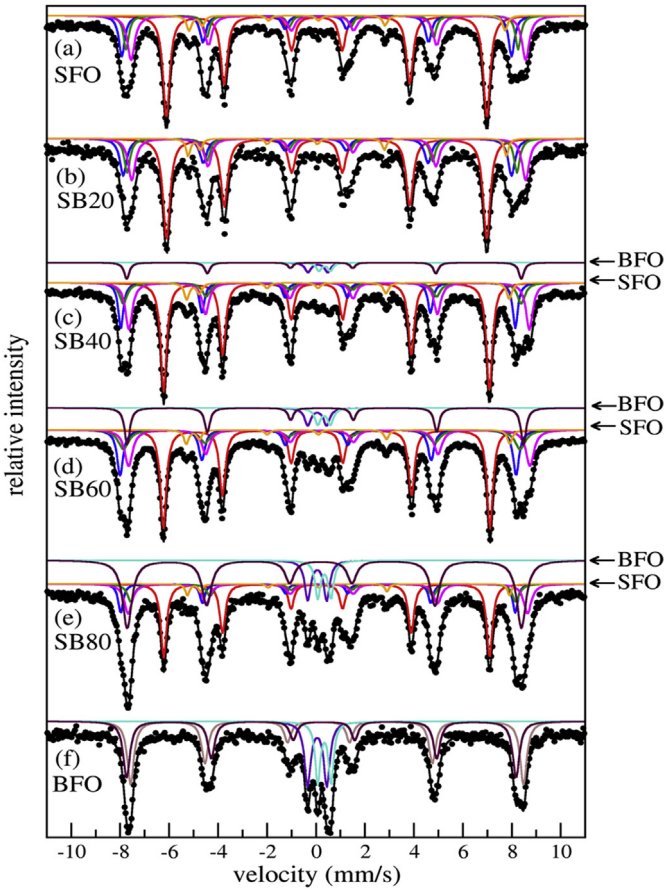

Fig. 9. Strontium Hexaferrite Mossbauer Spectrum $SrFe_{12}O_{19}$ added with $BiFeO_3$ in the proportions of 20, 40, 60 and 80 wt%.

Table 4
Hyperfine parameters obtained for the SFO - BFO composites measured at room temperature.

Sample	Model/Área	Site	Γ(mm/s)	δ(mm/s)	Δ (mm/s)	$^{B}HF^{(T)}$
SFO	SFO/100%	12k	0.323	0.346	0.393	40.6
		4f1	0.289	0.122	0.039	49.4
		4f2	0.260	0.321	0.081	49.7
		2a	0.360	0.498	0.237	50.0
		2b	0.235	0.291	2.184	40.0
BFO	BFO/100%	sext1	0.327	0.391	0.343	49.8
		sext2	0.333	0.383	−0.110	49.4
		dub-t	0.301	0.161	0.785	
		dub-o	0.253	0.345	0.546	
SB20	SFO/100%	12k	0.343	0.348	0.393	40.6
		4f1	0.338	0.134	0.070	49.2
		4f2	0.285	0.313	0.094	49.4
		2a	0.350	0.493	0.276	49.9
		2b	0.206	0.266	2.245	40.3
SB40	SFO/91.6%	12k	0.295	0.348	0.393	41.3
		4f1	0.250	0.157	0.076	50.0
		4f2	0.381	0.348	0.034	50.4
		2a	0.337	0.491	0.312	50.7
		2b	0.249	0.288	2.264	40.9
	BFO/8.4%	sext	0.253	0.392	0.102	50.0
		dub-t	0.291	0.186	0.805	
		dub-o	0.254	0.465	0.468	
SB60	SFO/82.8%	12k	0.290	0.350	0.397	41.4
		4f1	0.299	0.166	0.064	50.2
		4f2	0.512	0.317	0.080	50.3
		2a	0.390	0.503	0.302	50.8
		2b	0.235	0.293	2.256	41.0
	BFO/17.2%	sext	0.256	0.425	0.135	50.2
		dub-t	0.308	0.160	0.769	
		dub-o	0.296	0.440	0.512	
SB80	SFO/53.4%	12k	0.284	0.347	0.402	41.3
		4f1	0.242	0.163	0.056	50.0
		4f2	0.348	0.372	0.078	48.8
		2a	0.378	0.472	0.247	50.6
		2b	0.192	0.319	2.242	40.8
	BFO/46.4%	sext	0.458	0.380	0.144	49.9
		dub-t	0.291	0.162	0.775	
		dub-o	0.261	0.453	0.537	

Γ = line width; δ = isomer shift; Δ = quadrupole splitting; BHF = hyperfine magnetic field.
Maximum uncertainties: Γ (0,04 mm/s); δ (0,01 mm/s); Δ (0,03 mm/s); BHF (0,1 T); area (2%).
12k and Sext1 are iron sites for SFO and BFO structures.

of 20, 40, 60, 80 wt% and the values of saturation magnetization (Ms), remanent magnetization (Mr) and coercive field (Hc) of all samples are shown in Table 3. The composite powders analyzed in the magnetization measurements were mixed and thermally treated at the same sintering temperature. The BFO sample presents a typical antiferromagnetic arrangement, which is in agreement with the literature and also exhibits a weak magnetism at room temperature due to its adjustment corresponding to a simple arrangement in which the magnetic moment of each Fe^{3+} atom is surrounded by antiparallel moments of six Fe^{3+} atoms [33]. The hysteresis loop profiles in Fig. 7 to all composites and SFO samples show deformations in magnetization curves. These deformations can be associated at inhomogeneity of powder, must probably present two domain as seen in works of Valadkhan [34], where this domains can be explained by no uniformity of powders generate two or more magnetic domains. This no uniformity can ben seen in the micrograph of the Fig. 8, where is possible to see grains sizes different along of the micrograph. In the micrographs of Fig. 8 also is possible to see that addition of BFO promotes the growth of composite grains. This growth explain the variation in the coercive field, which reached a maximum value for the sample SB40 (Hc = −4.13 KOe). This correlation is demonstrate in Akbarzadeh's work [35] where there is a specific grain size with only one domain that shows higher coercivity. Above this grain size multi domains arise reducing coercivity. Thus the decreasing of coercivity presented above SB40 can be explained by the micrograph showed in Fig. 8, where the growth of grain favors the decreasing coercivity (multidomains) and there is great contribution of the antiferromagnetic phase of the BFO. For concentrations above SB40, the Hc follows the expected decreasing values due to the antiferromagnetic domains of the BFO. Another parameters obtained by hysteresis loop as Mr and Ms presented behavior expected for BFO addition, i.e., decreasing values with addition of antiferromagnetic phase.

Fig. 9 shows room temperature ^{57}Fe Mössbauer spectra (MS) for all samples. Hyperfine parameters obtained from best fits to the data are shown in Table 4. The Mössbauer spectrum of SFO is shown in Fig. 8-a. The structure of M-type hexagonal ferrites such as $SrFe_{12}O_{19}$ presents five distinct Fe^{3+} sites: three octahedral sites (12k, 2a, and 4f2), one tetrahedral site (4f1), and one trigonal bipyramidal site (2b) [36]. This structure results in a complex Mössbauer spectrum composed of five sub-spectra corresponding to each nonequivalent crystallographic site. There is a wide range of values reported for the hyperfine parameters of SFO, and thus the values found here are consistent with the literature [4,37–41]. The Mössbauer spectrum of BFO is shown in Fig. 8-f. The best fit was achieved with two Fe^{3+} sextets attributed to two distinct iron sites in the $BiFeO_3$ rhombohedral structure [42,43] and two Fe^{3+} doublets attributed to tetrahedral and octahedral iron in the orthorhombic $Bi_2Fe_4O_9$ structure [42,44]. These fitting models are hereafter referred to as SFO and BFO models.

The presence of BFO in the SB20 composite did not introduce a significant modification in the Mössbauer spectrum showed in Fig. 8-b. The best fit to the SB20 spectrum was achieved using the SFO model alone with consistent hyperfine parameters. The SB40, SB60, SB80 samples were fitted using a combination of both SFO and BFO models as can be seen in Fig. 8-c to 8-e. Attempts to include both $BiFeO_3$ sextets from the BFO model did not yield stable fits, therefore a single sextet was used together with the two $Bi_2Fe_4O_9$ doublets and the SFO model. All hyperfine parameters are consistent with the literature and with the SFO and BFO fits. The relative spectral area taken by the SFO model varied from 91.6% to 53.4% which is consistent with the decreasing amount of SFO in each sample of the series.

4. Conclusions

The syntheses of SFO and BFO were performed with success by solid-state reaction and these phases were confirmed in composites by XRD where the diffractograms showed only theses phases without spurious phases. The measured dielectric and electric properties demonstrate the improvement of thermal-stability of composites. The thermal-activated process of composites showed few oscillations compared to main phases. The Nyquist plot shows one arc fitted only one association of R-CPE due to the electric response of ceramic grains. The Mössbauer spectroscopy showed the iron sites characteristics of BFO and SFO as founded in the literature. The hysteresis loops showed one increase of Hc for SB20 and SB40 due to the increase of powder grains of theses samples, it demonstrates to be hard than SFO ferrite. The composites were studied with the most varied techniques for understanding the electrical, dielectric and magnetic properties, with their intended applications being for electronic devices, antennas, and devices that require control of the level of magnetic radiation among others.

Acknowledgments

The authors are grateful to CNPq, CAPES (Brazilian Agencies) and the US Air Force Office of Scientific Research (AFOSR) (FA9550-16-1-0127) for providing financial support.

References

[1] M.R. Meshram, N.K. Agrawal, B. Sinha, P.S. Misra, Transmission line modeling (TLM) for evaluation of absorption in ferrite based multi layer microwave absorber, in: TENCON 2003. Conf. Converg. Technol. Asia-Pacific Reg., Allied Publishers Pvt. Ltd, n.d.: pp. 626–630. doi:10.1109/TENCON.2003.1273246.
[2] M. Pardavi-Horvath, Microwave applications of soft ferrites, J. Magn. Magn Mater. 215–216 (2000) 171–183, https://doi.org/10.1016/S0304-8853(00)00106-2.
[3] K.H.J. Buschow, New developments in hard magnetic materials, 1991, https://doi.org/10.1088/0034-4885/54/9/001. Netherlands.
[4] P. Lampen-Kelley, A.S. Kamzin, K.E. Romachevsky, D.T.M. Hue, H.D. Chinh, H. Srikanth, M.H. Phan, Mössbauer spectroscopy studies of phase evolution in SrFe12O19/La0.5Ca0.5MnO3 composites, J. Alloys Compd. 636 (2015) 323–328, https://doi.org/10.1016/j.jallcom.2015.02.172.
[5] F.M.M. Pereira, A.S.B. Sombra, A review on BaxSr1-xFe12O19 hexagonal ferrites for use in electronic devices, Solid State Phenom. 202 (2013) 1–64, https://doi.org/10.4028/www.scientific.net/SSP.202.1.
[6] F.M.M. Pereira, R.S.T.M. Sohn, H.O. Rodrigues, G.F.M.P. Junior, K.R.B. Theophilo, M.J.S. Rocha, M.A.S. Silva, A.S.B. Sombra, Experimental and numerical investigation of a magnetic resonator antenna based on the M-type hexaferrite (BaxSr1â^'xFe12O19), Microw. Opt. Technol. Lett. 52 (2010) 452–458, https://doi.org/10.1002/mop.24931.
[7] G. Mu, H. Shen, J. Qiu, M. Gu, Microwave absorption properties of composite powders with low density, Appl. Surf. Sci. 253 (2006) 2278–2281, https://doi.org/10.1016/j.apsusc.2006.04.021.
[8] J. Qiu, Q. Zhang, M. Gu, H. Shen, Effect of aluminum substitution on microwave absorption properties of barium hexaferrite, J. Appl. Phys. 98 (2005), 103905, https://doi.org/10.1063/1.2135412.
[9] F. ur Raheem, M.A. Khan, A. Majeed, A. Hussain, M.F. Warsi, M.N. Akhtar, Structural, spectral, electrical, dielectric and magnetic properties of Yb doped SrNiCo-X hexagonal nano-structured ferrites, J. Alloys Compd. 708 (2017) 903–910, https://doi.org/10.1016/j.jallcom.2017.03.040.
[10] C. Liu, X. Liu, S. Feng, K.M.U. Rehman, M. Li, C. Zhang, H. Li, X. Meng, Microstructure and magnetic properties of M-type strontium hexagonal ferrites with Y-Co substitution, J. Magn. Magn Mater. 436 (2017) 126–129, https://doi.org/10.1016/j.jmmm.2017.04.040.
[11] A.A. Al-Ghamdi, F.S. Al-Hazmi, L.S. Memesh, F.S. Shokr, L.M. Bronstein, Evolution of the structure, magnetic and optical properties of Ni 1−x Cu x Fe 2 O 4 spinel ferrites prepared by soft mechanochemical method, J. Alloys Compd. 712 (2017) 82–89, https://doi.org/10.1016/j.jallcom.2017.04.052.
[12] M.N. Rahaman, Ceramic Processing and Sintering, second ed., 2003. Missouti, U.S.A.
[13] C.C. Yang, Y.J. Gung, C.C. Shih, W.C. Hung, K.H. Wu, Synthesis, infrared and microwave absorbing properties of (BaFe12O19+BaTiO3)/polyaniline composite, J. Magn. Magn Mater. 323 (2011) 933–938, https://doi.org/10.1016/j.jmmm.2010.11.072.
[14] O. Akman, H. Kavas, A. Baykal, Z. Durmus, B. Aktaş, H. Sözeri, Microwave absorption properties of BaFe12O19-TiO2 composite coated with conducting

polymer, J. Supercond. Nov. Magnetism 26 (2013) 1369–1373, https://doi.org/10.1007/s10948-012-1884-7.
[15] A.D.S.B. Costa, M.C. Romeu, R.C.S. Costa, T.S.M. Fernandes, F.W.D.O. Amarante, M.A.S. da Silva, G.D. Saraiva, A.S.B. Sombra, High thermal stability of microwave dielectric properties of CaTi 1-x (Nb 1/2 Fe 1/2) x O 3 ceramics, J. Adv. Dielect. 1 (2011) 417–427, https://doi.org/10.1142/S2010135X11000501.
[16] A.D.S. Bruno Costa, D.G. Sousa, R.C.S. Costa, F.W. de O. Amarante, T.S.M. Fernandes, G.D. Saraiva, M.A.S. da Silva, A.S.B. Sombra, High thermal stability of the microwave dielectric properties of CaTi 1− x (Nb 2/3 Li 1/3) x O 3−δ alloys, Phys. Scr 84 (2011) 55701, https://doi.org/10.1088/0031-8949/84/05/055701.
[17] L.S. Oliveira, D.X. Gouveia, M.A.S. Silva, A.S.B. Sombra, Study of the performance of dielectric resonator antennas based on the matrix composite of Al 2 O 3-CaTiO 3, Microw. Opt. Technol. Lett. 57 (2015) 963–969, https://doi.org/10.1002/mop.28999.
[18] R.V.B. Campos, C.L. Bezerra, L.N.L. Oliveira, D.X. Gouveia, M.A.S. Silva, A.S.B. Sombra, A study of the dielectric properties of Al2O3−TiO2 composite in the microwave and RF regions, J. Electron. Mater. 44 (2015) 4220–4226, https://doi.org/10.1007/s11664-015-3958-3.
[19] R.G.M. Oliveira, D.B. Freitas, M.C. Romeu, M.A.S. Silva, A.J.M. Sales, A.C. Ferreira, J.M.S. Filho, A.S.B. Sombra, Design and simulation of Na2Nb4O11 dielectric resonator antenna added with Bi2O3 for microwave applications, Microw. Opt. Technol. Lett. 58 (2016) 1211–1217, https://doi.org/10.1002/mop.29765.
[20] J.E.V. de Morais, R.G.M. de Oliveira, A.J.N. de Castro, J.C. Sales, M.A.S. Silva, J.C. Goes, M.M. Costa, A.S.B. Sombra, Dielectric study in the microwave range for ceramic composites based on Sr2CoNbO6 and TiO2 mixtures, J. Electron. Mater. 46 (2017) 5193–5200, https://doi.org/10.1007/s11664-017-5541-6.
[21] M.T. Sebastian, M.A.S. Silva, A.S.B. Sombra, Measurement of microwave dielectric properties and factors affecting them, in: Microw. Mater. Appl. 2V Set, John Wiley & Sons, Ltd, Chichester, UK, 2017, pp. 1–51, https://doi.org/10.1002/9781119208549.ch1.
[22] H.O. Rodrigues, G.F.M. Pires Junior, A.J.M. Sales, P.M.O. Silva, B.F.O. Costa, P. Alcantara, S.G.C. Moreira, A.S.B. Sombra, BiFeO3 ceramic matrix with Bi2O3 or PbO added: Mössbauer, Raman and dielectric spectroscopy studies, Phys. B Condens. Matter 406 (2011) 2532–2539, https://doi.org/10.1016/j.physb.2011.03.050.
[23] M. Čebela, D. Zagorac, K. Batalović, J. Radaković, B. Stojadinović, V. Spasojević, R. Hercigonja, BiFeO3 perovskites: a multidisciplinary approach to multiferroics, Ceram. Int. 43 (2017) 1256–1264, https://doi.org/10.1016/j.ceramint.2016.10.074.
[24] H.O. Rodrigues, A.J.M. Sales, G.F.M.P. Junior, J.S. Almeida, M.A.S. Silva, A.S.B. Sombra, Experimental and numerical investigation of dielectric resonator antenna based on the BiFeO3 ceramic matrix added with Bi2O3 or PbO, J. Alloys Compd. 576 (2013) 324–331, https://doi.org/10.1016/j.jallcom.2013.06.009.
[25] T. Tong, J. Chen, D. Jin, J. Cheng, Preparation and gas sensing characteristics of BiFeO 3 crystallites, Mater. Lett. 197 (2017) 160–162, https://doi.org/10.1016/j.matlet.2017.03.091.
[26] X.-Z. Yuan, C. Song, H. Wang, J. Zhang, Electrochemical Impedance Spectroscopy in PEM Fuel Cells, Springer London, London, 2010, https://doi.org/10.1007/978-1-84882-846-9.
[27] A.K. Jonscher, The “universal” dielectric response, Nature 267 (1977) 673–679, https://doi.org/10.1038/267673a0.
[28] D.G.R. William, D. Callister Jr., An Introduction, Mater. Sci. Eng. (2009).
[29] J. Bashir, R. Shaheen, Structural and complex AC impedance spectroscopic studies of A2CoNbO6 (A = Sr, Ba) ordered double perovskites, Solid State Sci. 13 (2011) 993–999, https://doi.org/10.1016/j.solidstatesciences.2011.02.003.
[30] K. Lily, K. Kumari, R.N.P. Prasad, Choudhary, Impedance spectroscopy of (Na0.5Bi0.5)(Zr0.25Ti0.75)O3 lead-free ceramic, J. Alloys Compd. 453 (2008) 325–331, https://doi.org/10.1016/j.jallcom.2006.11.081.
[31] A.M. Abo El Ata, S.M. Attia, Dielectric dispersion of Y-type hexaferrites at low frequencies, J. Magn. Magn Mater. 257 (2003) 165–174, https://doi.org/10.1016/S0304-8853(02)00446-8.
[32] D.J. Nicolin, D.F. Rossoni, L.M.M. Jorge, Study of uncertainty in the fitting of diffusivity of Fick's second law of diffusion with the use of bootstrap method, J. Food Eng. 184 (2016) 63–68, https://doi.org/10.1016/j.jfoodeng.2016.03.024.
[33] J. De Sitter, C. Dauwe, E. De Grave, A. Govaert, On the mossbauer parameters in BiFeO3, Solid State Commun. 18 (1976) 645–646, https://doi.org/10.1016/0038-1098(76)91502-7.
[34] S. Valadkhan, K. Morris, A. Khajepour, Review and comparison of hysteresis models for magnetostrictive materials, J. Intell. Mater. Syst. Struct. 20 (2009) 131–142, https://doi.org/10.1177/1045389X08093563.
[35] A. Akbarzadeh, M. Samiei, S. Davaran, Magnetic nanoparticles: preparation, physical properties, and applications in biomedicine, Nanoscale Res. Lett. 7 (2012) 144, https://doi.org/10.1186/1556-276X-7-144.
[36] P.M. Rao, A. Gérard, F. Grandjean, A mössbauer study of the effects of the substitution of Fe by Cr in SrFe12O19, Phys. Status Solidi 54 (1979) 529–536, https://doi.org/10.1002/pssa.2210540213.
[37] S.K. Chawla, P. Kaur, R.K. Mudsainiyan, S.S. Meena, S.M. Yusuf, Effect of Fuel on the synthesis, structural, and magnetic properties of m-type hexagonal SrFe12O19 nanoparticles, J. Supercond. Nov. Magnetism 28 (2015) 1589–1599, https://doi.org/10.1007/s10948-014-2893-5.
[38] B.J. Evans, F. Grandjean, A.P. Lilot, R.H. Vogel, A. Gérard, 57Fe hyperfine interaction parameters and selected magnetic properties of high purity MFe12O19 (M=Sr, Ba), J. Magn. Magn Mater. 67 (1987) 123–129, https://doi.org/10.1016/0304-8853(87)90728-1.
[39] N. Chen, K. Yang, M. Gu, Microwave absorption properties of La-substituted M-type strontium ferrites, J. Alloys Compd. 490 (2010) 609–612, https://doi.org/10.1016/j.jallcom.2009.10.116.
[40] J.H. de Araújo, J.M. Soares, M.F. Ginani, F.L.A. Machado, J.B.M. da Cunha, Mössbauer and magnetic study of nanocrystalline strontium hexaferrite prepared by an ionic coordination reaction technique, J. Magn. Magn Mater. 343 (2013) 203–207, https://doi.org/10.1016/j.jmmm.2013.04.077.
[41] A. Ghasemi, V. Šepelák, Correlation between site preference and magnetic properties of substituted strontium ferrite thin films, J. Magn. Magn Mater. 323 (2011) 1727–1733, https://doi.org/10.1016/j.jmmm.2011.02.010.
[42] D. Maurya, H. Thota, A. Garg, B. Pandey, P. Chand, H.C. Verma, Magnetic studies of multiferroic Bi 1− x Sm x FeO 3 ceramics synthesized by mechanical activation assisted processes, J. Phys. Condens. Matter 21 (2009) 26007, https://doi.org/10.1088/0953-8984/21/2/026007.
[43] V.F. Freitas, H.L.C. Grande, S.N. de Medeiros, I.A. Santos, L.F. Cótica, A.A. Coelho, Structural, microstructural and magnetic investigations in high-energy ball milled BiFeO3 and Bi0.95Eu0.05FeO3 powders, J. Alloys Compd. 461 (2008) 48–52, https://doi.org/10.1016/j.jallcom.2007.07.069.
[44] E. Kostiner, G.L. Shoemaker, Mössbauer effect study of Bi2Fe4O9, J. Solid State Chem. 3 (1971) 186–189, https://doi.org/10.1016/0022-4596(71)90025-9.